A process-based framework for quantifying the atmospheric preconditioning of surface triggered convection

Ahmed B. Tawfik[1] and Paul A. Dirmeyer[1]

[1]Center for Ocean-Land-Atmosphere Studies
George Mason University
4400 University Drive, Mail Stop 6C5
Fairfax, VA 22030, USA
Email: abtawfik@cola.iges.org

Abstract

Here we introduce the heated condensation framework, which contains a suite of variables for isolating the atmospheric boundary state from local surface forcing. The buoyant condensation level (BCL) and buoyant mixing temperature (θ_{BM}) quantify the degree to which the atmosphere is preconditioned for moist convection and can be calculated for any time of day or year using standard vertical profiles of temperature and humidity. Unlike the lifted condensation level and convective inhibition, the BCL is constructed through incremental mixing from the surface rather than lifting a hypothetical parcel. In this regard, the BCL represents a conserved condensation level diagnostic inherent to a given profile. The BCL and θ_{BM} are shown to be applicable over a range of climate regimes, and responds to synoptic and mesoscale forcings, illustrating its broader utility. A suite of variables relating the BCL directly to surface fluxes is also introduced.

1. Introduction

The role of the land surface in triggering and amplifying precipitation has been the focus of recent research [e.g., *Zhang and Klein*, 2010; *Findell et al.*, 2011; *Gentine et al.*, 2013b; *Santanello et al.*, 2013] reflecting the ability of soil moisture states to affect precipitation [*Fennessy and Shukla*, 1999; *Betts*, 2004]. This coupling has been most strongly identified over semi-arid regions [*Guo et al.*, 2006; *Koster et al.*, 2006] due to greater flux sensitivity and variability [*Dirmeyer*, 2011]. Thus the potential exists for improved seasonal predictability by better representation of soil moisture [*Guo et al.*, 2011; *Koster et al.*, 2011]. To better understand the impact of surface forcing on precipitation, atmospheric preconditioning (the synoptic background state) must be quantified in a manner physically consistent with land-boundary layer interactions.

The growth of the planetary boundary layer (PBL) throughout the day is a function of the interplay between surface fluxes, the vertical profile of the overlaying atmosphere, and advection [*Betts*, 2000, 2009; *Berg and Stull*, 2004]. As the surface is heated by incident radiation, near-surface air becomes more buoyant. Rising air mixes upward, homogenizing the air within the growing PBL while entraining relatively dry air from the free troposphere [*Berg and Stull*, 2004; *Betts*, 2009]. This results in near-constant potential temperature and water vapor mixing ratio profiles, and also serves to define the PBL height itself. Clouds may form if the top of the PBL is sufficiently cooled [*Gentine et al.*, 2013a; *Zhang and Klein*, 2013], potentially producing precipitation [*Haiden*, 1997].

Treating land-atmosphere interactions as a cascade of steps from the surface

49 to the atmosphere allows the relative importance of different processes to be
50 isolated [*Seneviratne et al.*, 2010; *Santanello et al.*, 2011]. Efforts have been made to
51 derive metrics for quantifying these particular steps [*De Ridder*, 1997; *Findell and*
52 *Eltahir*, 2003; *Ek and Holtslag*, 2004; *Santanello et al.*, 2009; *van Heerwaarden et al.*,
53 2010; *Ferguson et al.*, 2012]. However, disentangling the large-scale forcing from
54 the local land surface forcing has been particularly difficult [*Berg and Stull*, 2004;
55 *Ferguson and Wood*, 2011]. Findell and Eltahir [2003] introduced a method using
56 morning soundings that identifies certain regimes where the land surface may
57 influence convective triggering. Although this method was robust over Illinois,
58 Ferguson and Wood [2011] had to modify thresholds to be suitable globally when
59 using remote sensing data. Other studies have quantified the free tropospheric
60 stability using temperature and specific humidity lapse rates above the PBL within
61 the context of convective triggering [*De Ridder*, 1997; *Ek and Holtslag*, 2004; *Gentine*
62 *et al.*, 2013b]. This is typically done using a "jump" criterion in a single-column
63 model where conserved fields (potential temperature and specific humidity) are
64 perturbed at the top of the mixed layer mimicking the transition to the free
65 troposphere. Conserved parcel metrics such as the lifted condensation level (LCL),
66 the level of free convection (LFC), and convective inhibition (CIN), have also been
67 used as diagnostics for identifying convective triggering [*Betts*, 2004; *Guichard et al.*,
68 2004; *Zhang and Klein*, 2010; *Santanello et al.*, 2011]. Santanello et al. [2011]
69 showed that when the LCL is below the PBL depth, convection may occur providing
70 a necessary but not sufficient condition for convective triggering. Gentine et al.
71 [2013b] used the difference between the mixed-layer and saturation equivalent

potential temperature above the inversion to diagnose the difference between active and forced convection.

These methods typically neglect the incremental growth of the PBL by one of two assumptions: 1) basing metrics on atmospheric states at arbitrary heights or 2) lifting a parcel from a certain height without allowing the parcel to mix with its surroundings. This is problematic especially on hourly timescales where LCL, LFC, and CIN are seen to vary substantially throughout the day [*Guichard et al.*, 2004; *Betts*, 2009], making it difficult for such metrics to identify a representative atmospheric background state with respect to convection.

Here we introduce a new diagnostic framework, the heated condensation framework (HCF), which defines the buoyant condensation level (BCL) and the buoyant mixing potential temperature (θ_{BM}). These two variables quantify how conditioned the atmosphere is to moist free convection due to surface heating. The HCF variables are calculated using standard meteorological soundings (specific humidity and temperature profiles) and may be calculated for any time of day. The framework produces a suite of other quantities that provide insight into the conditions necessary for triggering convection, but the primary focus here will be on variables that quantify the atmospheric background state (e.g. the BCL and θ_{BM}) with brief mention of how to calculate HCF variables related to surface fluxes. These HCF surface flux variables will be more thoroughly explored in a subsequent paper.

2. Heated Condensation Framework

The BCL is defined as the level at which saturation would occur through

95 buoyant mixing alone due to sensible heating from the surface. Alternatively, the
96 BCL is the height the growing PBL needs to reach for saturation to occur without the
97 addition or removal of moisture from the column. To find the BCL, a hypothetical
98 boundary layer is constructed using the vertical profiles of potential temperature, θ,
99 and specific humidity, q. This is done in four steps illustrated by the thermodynamic
100 profiles in Figure 1. 1) First, increase the near-surface potential temperature (θ_{2m})
101 by a small increment, $\Delta\theta$ (Figure 1a). 2) Find the height where the perturbed near-
102 surface parcel ($\theta_{2m} + \Delta\theta$) is neutrally buoyant (Figure 1b). 3) Mix the specific
103 humidity profile from the surface to the level of neutral buoyancy returning a
104 constant mixed layer humidity, q_{mix} (Figure 1b). 4) Upon mixing, check if saturation
105 occurs at the top of the potential mixed level (PML) by comparing q_{mix} and the
106 saturation specific humidity at the PML, $q^*(\theta_{pml})$. The sequence is repeated until
107 saturation occurs (Figure 1c). Note that the BCL is a special case of the PML when
108 saturation is reached (e.g. $q^*(\theta_{pml}) - q_{mix} = 0$), where the sum of all $\Delta\theta$ increments
109 required to attain the BCL is the total energy deficit, θ_{def} (Figure 1c). Unlike parcel-
110 derived metrics (LCL, LFC, CAPE, and CIN) that change for a given profile depending
111 on the parcel selected for lifting, the BCL is an inherent property of a given profile
112 that does not vary unless the temperature and humidity profiles change. This
113 makes the BCL height independent from the initial θ_{2m} and is therefore insensitive
114 to the starting temperature (e.g. time of day) as long as the q and T profiles do not
115 change.

116 Other useful quantities can also be derived within this framework.
117 Specifically, the buoyant mixing potential temperature, θ_{BM}, identifies the near-

surface potential temperature required to attain the BCL height ($\theta_{BM} = \theta_{2m} + \theta_{def}$). Before the BCL height is reached (step 4; Figure 1b) a moisture deficit at the top of the potential mixed layer (PML) can be calculated ($q_{def} = q^*(\theta_{pml}) - q_{mix}$). θ_{def} and q_{def} are both easily translated into time integrated surface flux units. For example, multiplying q_{def} by the column density (ρ_h) of the potential mixed level returns the amount of moisture (either through evapotranspiration or advection) needed to be injected into the PML for saturation to occur at a given potential temperature. Similarly, θ_{def} multiplied by the specific heat capacity (c_p) and mean column density (ρ_h) returns the necessary sensible heat energy. Therefore during each $\Delta\theta$ increment the amount of heat input ($c_p\rho_h\Delta\theta$) and moisture input ($\rho_h q_{def}$) necessary for saturation can be quantified.

3. Data

3.1 Integrated Global Radiosonde Archive

Vertical profiles of temperature and humidity are provided by the Integrated Global Radiosonde Archive [IGRA; *Durre et al.*, 2006]. The IGRA is a global quality controlled sounding dataset with the greatest spatial and temporal coverage over the United States and Europe typically measuring at 0000UTC and 1200UTC. Here we focus on the continental United States (23-50°N and 130-66°W) with data from January 1970 to June 2013 where available. To be used, each sounding must have at least 8 levels with 60% soundings for a station recording more than 20 levels. Additionally, soundings are filtered to include only those that reach 600 hPa to ensure sufficient vertical resolution when calculating the HCF variables. Finally,

stations must have at least 500 soundings to be included in the climatological analysis (Section 4.2).

3.2 Rapid Refresh

One week of output (July 23rd to July 30th 2012) from the Rapid Refresh (RAP) forecast model system, the next generation of the Rapid Update Cycle (RUC) [*Benjamin et al.*, 2004], is used to illustrate the utility of the HCF on hourly timescales. RAP is an operational short-range weather forecast system using the regional Weather Research and Forecast model (WRF-ARW version 3.3) [*Skamarock et al.*, 2008] to produce hourly forecasts over North America. The RAP model has 50 vertical levels up to 10 hPa and a horizontal grid spacing of 13 km. Here we use output from the first forecast hour providing a close representation of the assimilated observations. Instantaneous vertical profiles of temperature, specific humidity, and cloud cover are used, in addition to total accumulated precipitation over the prior hour.

4. Results

4.1 Event Application of HCF

A maritime (Miami, Florida) and a continental (Amarillo, Texas) radiosonde station are examined for a week in July spanning days of year (DOY) 205-212 (Figure 2). Miami and Amarillo are among the stations in Figure 3. θ_{2m} is compared against θ_{BM} instead of comparing the BCL and PBL heights to avoid uncertainties regarding definition and calculation of boundary layer height [*Seidel et al.*, 2010;

164 *LeMone et al.*, 2013]. Note that the θ_{BM}- θ_{2m} comparison provides the same
165 information regarding the departure from saturation as the BCL-PBL comparison
166 except in a different parameter space.

167 Although Miami and Amarillo represent two distinct climate regimes, at both
168 stations precipitation and cloud cover are absent on days when daytime θ_{BM} is much
169 larger than θ_{2m} (Figure 2). Further, θ_{BM} calculated from RAP is shown to closely
170 follow θ_{BM} calculated from morning (1200UTC) and afternoon (0000UTC) IGRA
171 observations, providing confidence in the hourly RAP output (Figure 2). For Miami,
172 θ_{BM} shows strong diurnal variations with a minimum of 300 K, typically during mid-
173 morning, and a maximum at night greater than 310 K. This suggests that there is a
174 strong diurnal change in low-level moisture consistent with a land-sea breeze (see
175 supplementary material for further discussion of the Miami land-sea breeze.)
176 Convection appears to be controlled by the rapid daytime decrease of θ_{BM} (e.g.
177 moistening of the large-scale background state and lowering BCL height) during this
178 week.

179 At Amarillo there is little diurnal variability in θ_{BM}, suggesting that the
180 atmospheric background state is not largely influenced by local surface forcing
181 during this week (Figure 2). Additionally, θ_{BM} rapidly increases during the evening
182 of DOY 209, during which time clear-sky conditions persist. This increase in θ_{BM}
183 occurred when a ridge developed over the central US producing an upper level high-
184 pressure system centered over northern Texas (see supplementary material for
185 further discussion.) However, there are times when clouds and precipitation occur
186 without a θ_{BM}- θ_{2m} intersection, namely at night for DOY 205-209. Because the HCF

187 is developed to diagnose convective triggering due to surface heating, nocturnal
188 precipitation events associated with eastward propagating mesoscale convective
189 complexes (MCCs) [*Moncrieff*, 2013] over the central US likely would not influence
190 θ_{BM} unless near-surface vertical profiles of q and θ were impacted. This is discussed
191 further in Section 5. Overall we see the ability of the HCF to capture the background
192 atmospheric state for non-precipitating transient synoptic systems (Amarillo high
193 pressure system) and changes in mesoscale circulation (Miami land-sea breeze.)
194
195 *4.2 BCL Height Climatology*
196 The mean and standard deviations of the BCL height are presented by season
197 over the US, using several decades of 1200UTC IGRA data (Figure 3). The lowest BCL
198 heights occur over the southeastern US and the highest values are over the
199 southwestern US during the summer months (JJA) with a gradual transition from
200 low to high values moving westward. The seasonal cycle of average BCL height is
201 strongest in the southern half of the US and east of the Rocky Mountains with a
202 winter (DJF) maximum between 3.8-5 km and a summer (JJA) minimum of 1.5-3.5
203 km. This is expected because convective activity typically peaks during the summer
204 months. Conversely, the seasonal cycle for the northwest US is weaker and has the
205 lowest BCL heights in DJF and highest in JJA. The Southwest shows almost no
206 seasonal variation in BCL height (Figure 3).
207 The pattern of BCL height variability (σ_{BCL}) does not change from fall (SON)
208 through spring (MAM). However, there is a strong reduction in variability that
209 occurs during JJA from the Southeast through the Plains and Rocky Mountains

(Figure 3). Furthermore, σ_{BCL} has the most pronounced seasonal cycle over the Southeast with the BCL height varying by more than 2.5 km from day-to-day in DJF and less than 1.5 km in JJA.

Considering the seasonal behavior of BCL height, locations where the land surface may play a role in triggering convection can be deduced and highlighted for further investigation. Focusing on JJA, the BCL height patterns can be qualitatively separated into three categories: areas where the BCL height is 1) low, making convection likely under most surface (soil moisture) conditions, 2) attainable under specific surface conditions making convection conditional on the land surface state, and 3) so high as to make moist convection unattainable. Note that these categories mirror the land-atmosphere regimes described by Findell and Eltahir [2003]; however, the BCL height has the advantage of summarizing the background state in a single metric without requiring the selection of arbitrary humidity or stability levels making the BCL height (or θ_{BM}) more globally applicable.

To provide an examination of the likelihood of convective triggering, the average θ_{def} is also presented (Figure 3), where smaller values represent a greater chance of triggering. The seasonal cycle is amplified when presented in terms of θ_{def}, with DJF requiring an increase of more than 28 K from the morning θ_{2m} (1200UTC) on average for most of the US and less than 18 K for JJA (Figure 3). As a first approximation for identifying the three regimes, terciles of the average θ_{def} across all stations and seasons were calculated, where values less than 16 K (~33rd percentile) represent the first regime, values between 16-23 K represent the second regime, and values greater than 23 K (~67th percentile) the third. The Southeast

and Gulf Coast would likely fall under the first regime because an increase in surface potential temperature of less than 16 K is required on average to trigger convection for JJA. The West Coast would lie in the third regime (convection unattainable over any surface) because morning (1200UTC) θ_{2m} would need to increase by more than 23 K to trigger convection. The Central Plains, typically identified as a land-atmosphere coupling hotspot [*Koster et al.*, 2006], and the Great Lakes region fall into the second regime, suggesting that convection may be favored if there is a sustained moisture source (through low-level moisture convergence or evapotranspiration) into the PBL or the surface is sufficiently dry making it capable of overcoming the 16-23 K temperature deficit (Figure 3). Station-specific parameters that influence the diurnal temperature range (such as vegetation type, soil moisture, and soil properties) could influence the boundary between the three regimes. To more rigorously categorize these regimes, the diurnal evolution of θ_{def} must be examined. However, IGRA observations do not provide sufficient hourly resolution to perform this analysis.

5. Discussion and Conclusions

A process-based diagnostic framework (HCF) is introduced to quantify the atmospheric background state within the context of land-boundary layer interactions. The HCF has advantages that make it useful for studying the impact of surface fluxes on convective triggering. First, the construction of the BCL height mimics the evolution of the convective boundary layer and initiation of convection to first order (Figure 1). Rather than lifting a hypothetical unmixed parcel, the HCF

256 constructs a hypothetical boundary layer by incrementally inputting heat at the
257 surface. Information regarding the atmospheric background state (via BCL height
258 and θ_{BM}) and surface energy interaction can be derived (using θ_{def} and q_{def}) that are
259 physically consistent with PBL development. The BCL height and θ_{BM} are diagnostic
260 properties of a given profile not subject to parcel selection bias. The BCL is similar to
261 the mixing condensation level (MCL), which has long been used for examining fog
262 [*Petterssen*, 1939] and marine stratocumulus [*Miller et al.*, 1998]. The primary
263 difference is that the MCL assumes wind-driven mixing of both the θ and q profiles,
264 whereas the BCL assumes buoyancy-driven mixing by perturbing θ_{2m} and mixing the
265 q profile. An analogy could also be drawn with the convective condensation level
266 (CCL); however, like the LCL, the CCL is calculated by lifting a parcel of water vapor
267 that does not mix with its surroundings, resulting in the same shortcomings
268 discussed above.

269 Another advantage is that an atmospheric background state can be calculated
270 during any time of day (Figure 2) or year (Figure 3). This allows for the evaluation
271 of land-atmosphere coupling on a hourly basis without having to remove weather
272 variability by time-averaging [cf., *Betts*, 2004; *Guo et al.*, 2006; *Koster et al.*, 2006].
273 The HCF may be easily applied because only temperature and humidity profiles are
274 required. The sensitivity of the HCF to vertical resolution needs to be examined
275 further, however, preliminary analysis shows that mean BCL height changes by less
276 than +/- 500m for 75% of 1200UTC soundings when the number of IGRA vertical
277 levels are halved. Additionally, when analyzing 1200UTC soundings BCL height
278 climatology (Figure 3), the difference in solar time across the US introduces biases

279 of less than 160 meters for most stations when using hourly RAP output from July
280 2012.

281 Similar to other column-derived metrics [*De Ridder*, 1997; *Findell and Eltahir*,
282 2003], a primary shortcoming of HCF is its inability to distinguish between transient
283 and locally-driven precipitation. Although it was shown to capture low-level
284 moisture advection (Figure 2), a passing precipitation event may rapidly lower the
285 BCL height through re-evaporation of precipitation within the PBL. This makes the
286 signal between re-evaporation and rapid low-level moisture convergence difficult to
287 determine without sub-hourly profiles or information of surrounding synoptic
288 conditions. Therefore, although the evolution of the atmospheric background state
289 is accurately captured, more information would be required to identify the specific
290 process. Combining BCL information with existing coupling diagnostics, such as the
291 LCL deficit representation of near-surface parcel forcing [*Santanello et al.*, 2011],
292 may help identify the role of the land surface in triggering and enhancing
293 convection.

294

295 *Acknowledgements*:
296 This work was supported by National Science Foundation grant 0947837 for Earth
297 System Modeling post-docs. We would like to thank Bert Holtslag, Kirsten Findell,
298 Craig Ferguson, Chiel van Heerwaarden, Alan Betts, Pierre Gentine, Randal Koster,
299 Joseph Santanello, and Michael Ek for their helpful comments that have truly
300 improved the quality of this manuscript.

301

References:

Benjamin, S. G. et al. (2004), An Hourly Assimilation Forecast Cycle: The RUC, *Mon. Weather Rev.*, *132*, 495, doi:10.1175/1520-0493(2004)132<0495:AHACTR>2.0.CO;2.

Berg, L. K., and R. B. Stull (2004), Parameterization of Joint Frequency Distributions of Potential Temperature and Water Vapor Mixing Ratio in the Daytime Convective Boundary Layer, *J. Atmospheric Sci.*, *61*(7), 813–828, doi:10.1175/1520-0469(2004)061<0813:POJFDO>2.0.CO;2.

Betts, A. K. (2000), Idealized Model for Equilibrium Boundary Layer over Land, *J. Hydrometeorol.*, *1*(6), 507–523, doi:10.1175/1525-7541(2000)001<0507:IMFEBL>2.0.CO;2.

Betts, A. K. (2004), Understanding Hydrometeorology Using Global Models, *Bull. Am. Meteorol. Soc.*, *85*(11), 1673–1688, doi:10.1175/BAMS-85-11-1673.

Betts, A. K. (2009), Land-surface-atmosphere coupling in observations and models, *J. Adv. Model. Earth Syst.*, *2*, doi:10.3894/JAMES.2009.1.4. [online] Available from: http://james.agu.org/index.php/JAMES/article/view/v1n4 (Accessed 13 September 2012)

Dirmeyer, P. A. (2011), The terrestrial segment of soil moisture–climate coupling, *Geophys. Res. Lett.*, *38*(16), L16702, doi:10.1029/2011GL048268.

Durre, I., R. S. Vose, and D. B. Wuertz (2006), Overview of the Integrated Global Radiosonde Archive, *J. Clim.*, *19*(1), 53–68, doi:10.1175/JCLI3594.1.

Ek, M. B., and A. A. M. Holtslag (2004), Influence of Soil Moisture on Boundary Layer Cloud Development, *J. Hydrometeorol.*, *5*(1), 86–99, doi:10.1175/1525-7541(2004)005<0086:IOSMOB>2.0.CO;2.

Fennessy, M. J., and J. Shukla (1999), Impact of Initial Soil Wetness on Seasonal Atmospheric Prediction, *J. Clim.*, *12*(11), 3167–3180, doi:10.1175/1520-0442(1999)012<3167:IOISWO>2.0.CO;2.

Ferguson, C. R., and E. F. Wood (2011), Observed Land–Atmosphere Coupling from Satellite Remote Sensing and Reanalysis, *J. Hydrometeorol.*, *12*(6), 1221–1254, doi:10.1175/2011JHM1380.1.

Ferguson, C. R., E. F. Wood, and R. K. Vinukollu (2012), A Global Intercomparison of Modeled and Observed Land–Atmosphere Coupling*, *J. Hydrometeorol.*, *13*(3), 749–784, doi:10.1175/JHM-D-11-0119.1.

Findell, K. L., and E. A. B. Eltahir (2003), Atmospheric Controls on Soil Moisture–Boundary Layer Interactions. Part I: Framework Development, *J.*

337 *Hydrometeorol.*, *4*(3), 552–569, doi:10.1175/1525-
338 7541(2003)004<0552:ACOSML>2.0.CO;2.

339 Findell, K. L., P. Gentine, B. R. Lintner, and C. Kerr (2011), Probability of afternoon
340 precipitation in eastern United States and Mexico enhanced by high
341 evaporation, *Nat. Geosci.*, *4*(7), 434–439, doi:10.1038/ngeo1174.

342 Gentine, P., A. K. Betts, B. R. Lintner, K. L. Findell, C. C. van Heerwaarden, and F.
343 D'Andrea (2013a), A Probabilistic Bulk Model of Coupled Mixed Layer and
344 Convection. Part II: Shallow Convection Case, *J. Atmospheric Sci.*, *70*(6), 1557–
345 1576, doi:10.1175/JAS-D-12-0146.1.

346 Gentine, P., A. A. M. Holtslag, F. D'Andrea, and M. Ek (2013b), Surface and
347 atmospheric controls on the onset of moist convection over land, *J.*
348 *Hydrometeorol.*, 130211131121003, doi:10.1175/JHM-D-12-0137.1.

349 Guichard, F. et al. (2004), Modelling the diurnal cycle of deep precipitating
350 convection over land with cloud-resolving models and single-column models,
351 *Q. J. R. Meteorol. Soc.*, *130*(604), 3139–3172, doi:10.1256/qj.03.145.

352 Guo, Z. et al. (2006), GLACE: The Global Land–Atmosphere Coupling Experiment.
353 Part II: Analysis, *J. Hydrometeorol.*, *7*(4), 611–625, doi:10.1175/JHM511.1.

354 Guo, Z., P. A. Dirmeyer, and T. DelSole (2011), Land surface impacts on subseasonal
355 and seasonal predictability, *Geophys. Res. Lett.*, *38*(24), L24812,
356 doi:10.1029/2011GL049945.

357 Haiden, T. (1997), An analytical study of cumulus onset, *Q. J. R. Meteorol. Soc.*,
358 *123*(543), 1945–1960, doi:10.1002/qj.49712354309.

359 Van Heerwaarden, C. C., J. Vilà-Guerau de Arellano, A. Gounou, F. Guichard, and F.
360 Couvreux (2010), Understanding the Daily Cycle of Evapotranspiration: A
361 Method to Quantify the Influence of Forcings and Feedbacks, *J.*
362 *Hydrometeorol.*, *11*(6), 1405–1422, doi:10.1175/2010JHM1272.1.

363 Koster, R. D. et al. (2006), GLACE: The Global Land–Atmosphere Coupling
364 Experiment. Part I: Overview, *J. Hydrometeorol.*, *7*(4), 590–610,
365 doi:10.1175/JHM510.1.

366 Koster, R. D. et al. (2011), The Second Phase of the Global Land–Atmosphere
367 Coupling Experiment: Soil Moisture Contributions to Subseasonal Forecast
368 Skill, *J. Hydrometeorol.*, *12*(5), 805–822, doi:10.1175/2011JHM1365.1.

369 LeMone, M. A., M. Tewari, F. Chen, and J. Dudhia (2013), Objectively Determined
370 Fair-Weather CBL Depths in the ARW-WRF Model and Their Comparison to
371 CASES-97 Observations, *Mon. Weather Rev.*, *141*(1), 30–54,
372 doi:10.1175/MWR-D-12-00106.1.

373 Miller, M. A., M. P. Jensen, and E. E. Clothiaux (1998), Diurnal Cloud and
374 Thermodynamic Variations in the Stratocumulus Transition Regime: A Case
375 Study Using In Situ and Remote Sensors, *J. Atmospheric Sci.*, *55*(13), 2294–
376 2310, doi:10.1175/1520-0469(1998)055<2294:DCATVI>2.0.CO;2.

377 Moncrieff, M. W. (2013), The Multiscale Organization of Moist Convection and the
378 Intersection of Weather and Climate, in *Climate Dynamics: Why Does Climate*
379 *Vary?*, edited by D.-Z. Sun and F. Bryan, pp. 3–26, American Geophysical
380 Union. [online] Available from:
381 http://onlinelibrary.wiley.com/doi/10.1029/2008GM000838/summary

382 Petterssen, S. (1939), Some Aspects of Formation and Dissipation of Fog, *Geofys.*
383 *Publ.*, *12*(10), 22.

384 De Ridder, K. (1997), Land surface processes and the potential for convective
385 precipitation, *J. Geophys. Res.*, *102*(D25), 30085, doi:10.1029/97JD02624.

386 Santanello, J. A., C. D. Peters-Lidard, S. V. Kumar, C. Alonge, and W.-K. Tao (2009), A
387 Modeling and Observational Framework for Diagnosing Local Land–
388 Atmosphere Coupling on Diurnal Time Scales, *J. Hydrometeorol.*, *10*(3), 577–
389 599, doi:10.1175/2009JHM1066.1.

390 Santanello, J. A., C. D. Peters-Lidard, and S. V. Kumar (2011), Diagnosing the
391 Sensitivity of Local Land–Atmosphere Coupling via the Soil Moisture–
392 Boundary Layer Interaction, *J. Hydrometeorol.*, *12*(5), 766–786,
393 doi:10.1175/JHM-D-10-05014.1.

394 Santanello, J. A., C. D. Peters-Lidard, A. Kennedy, and S. V. Kumar (2013), Diagnosing
395 the Nature of Land–Atmosphere Coupling: A Case Study of Dry/Wet
396 Extremes in the U.S. Southern Great Plains, *J. Hydrometeorol.*, *14*(1), 3–24,
397 doi:10.1175/JHM-D-12-023.1.

398 Seidel, D. J., C. O. Ao, and K. Li (2010), Estimating climatological planetary boundary
399 layer heights from radiosonde observations: Comparison of methods and
400 uncertainty analysis, *J. Geophys. Res. Atmospheres*, *115*(D16), n/a–n/a,
401 doi:10.1029/2009JD013680.

402 Seneviratne, S. I., T. Corti, E. L. Davin, M. Hirschi, E. B. Jaeger, I. Lehner, B. Orlowsky,
403 and A. J. Teuling (2010), Investigating soil moisture–climate interactions in a
404 changing climate: A review, *Earth-Sci. Rev.*, *99*(3–4), 125–161,
405 doi:10.1016/j.earscirev.2010.02.004.

406 Skamarock, W. C., J. B. Klemp, J. Dudhia, D. O. Gill, D. M. Barker, M. G. Duda, X.-Y.
407 Huang, W. Wang, and J. G. Powers (2008), A Description of the Advanced
408 Research WRF Version 3, *NCAR Tech. Note*, *NCAR/TN–475+STR*.

409 Zhang, Y., and S. A. Klein (2010), Mechanisms Affecting the Transition from Shallow
410 to Deep Convection over Land: Inferences from Observations of the Diurnal
411 Cycle Collected at the ARM Southern Great Plains Site, *J. Atmospheric Sci.*,
412 *67*(9), 2943–2959, doi:10.1175/2010JAS3366.1.

413 Zhang, Y., and S. A. Klein (2013), Factors Controlling the Vertical Extent of Fair-
414 Weather Shallow Cumulus Clouds over Land: Investigation of Diurnal-Cycle
415 Observations Collected at the ARM Southern Great Plains Site, *J. Atmospheric*
416 *Sci.*, *70*(4), 1297–1315, doi:10.1175/JAS-D-12-0131.1.

417

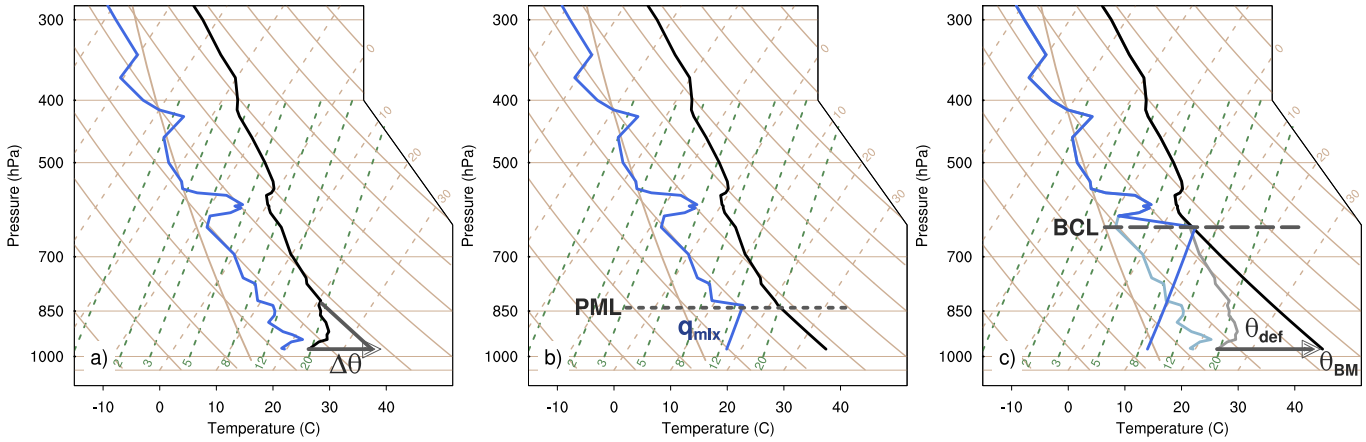

418 Figure 1: Thermodynamic profiles (e.g. skewT-logP diagrams) of temperature
419 (black) and dew point temperature (blue) illustrating the steps for calculating the
420 buoyant condensation level (BCL), buoyant mixing temperature (θ_{BM}), and mixed
421 layer specific humidity (q_{mix}). Dashed green lines represent constant mixing ratio
422 lines, dashed tan lines represent isotherms and solid tan lines are dry adiabats. a)
423 describes the first step where θ_{2m} is perturbed by some increment, $\Delta\theta$. b) identifies
424 the height, the potential mixed level (PML), where the perturbed surface parcel (θ_{2m}

425 + $\Delta\theta$) is neutrally buoyant and the humidity profile is mixed from the PML to the
426 surface. c) θ_{2m} is perturbed until saturation occurs at the PML and the level is
427 identified as the BCL. θ_{def} is the total potential temperature increment necessary to
428 reach θ_{BM} from the initial θ_{2m}. Faint blue and grey lines in c) refer to the
429 unperturbed profile shown in a) as a reference.
430

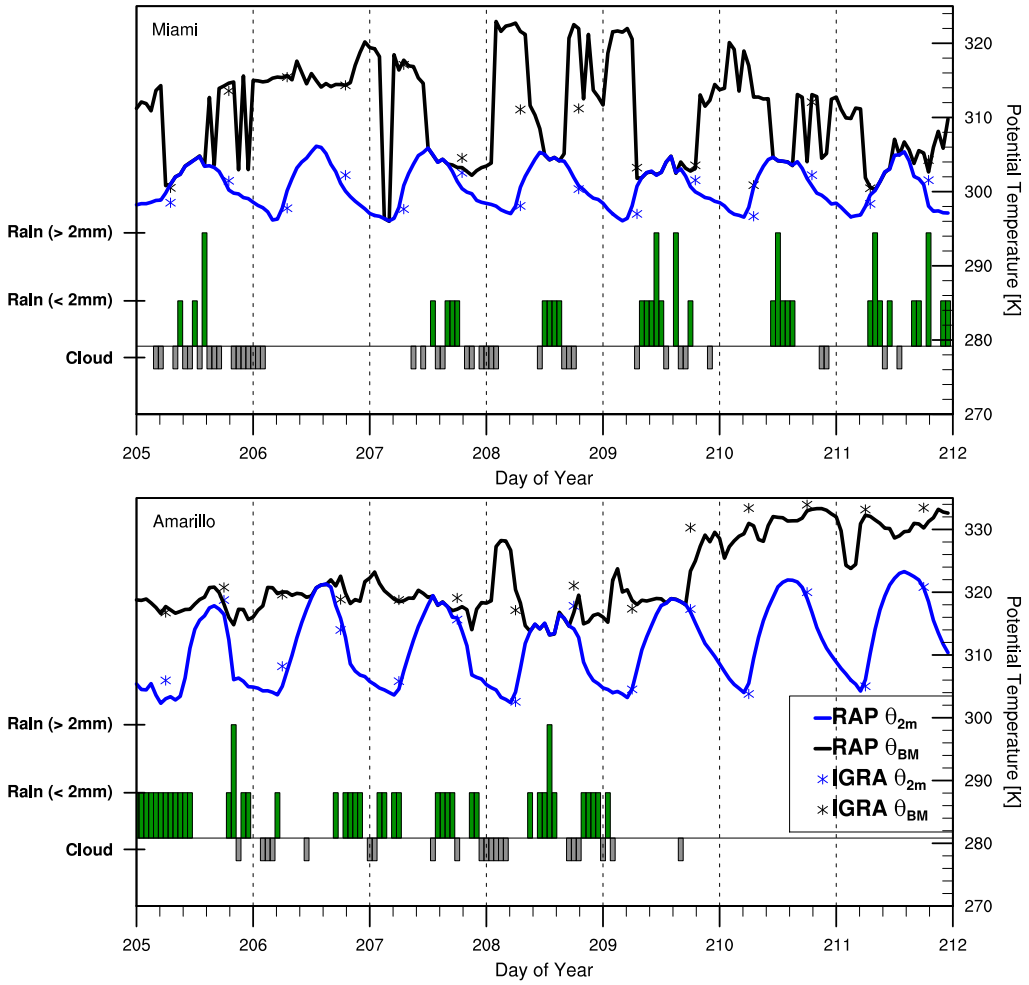

431 Figure 2: Hourly buoyant mixing potential temperature, θ_{BM}, from RAP (black line)
432 and IGRA soundings (black asterisk) compared against hourly 2-meter potential
433 temperature from RAP (blue line) and first sounding level potential temperature
434 from IGRA (blue asterisk) from July 23rd to July 30th 2012 for Miami, Florida
435 (25.75°N and 80.83°W) and Amarillo, Texas (35.23°N and 101.70°W). RAP
436 precipitation (green bars) is binned by hourly accumulations greater than 2 mm and
437 less than 2 mm. Grey bars represent the presence of non-precipitating clouds lower
438 than 8 km above the ground also from RAP. Stations are identified in Figure 3.
439

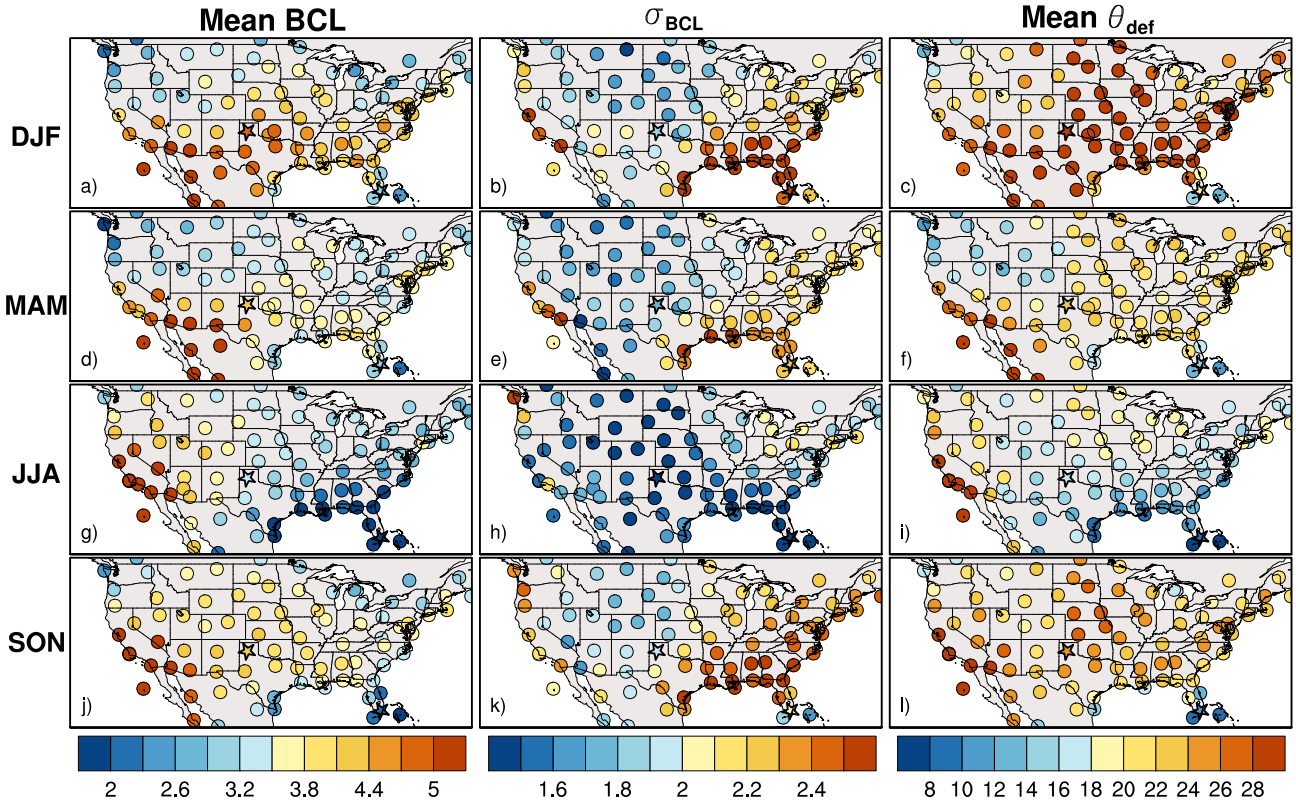

440 Figure 3: Seasonal cycle of average buoyant condensation level (BCL in km; left),
441 intra-seasonal variability of the BCL (σ_{BCL} in km; middle), and average additional
442 temperature increase necessary to trigger convection (θ_{def} in K; right) at IGRA
443 stations for 1200UTC soundings. The stars represent the Amarillo, Texas and
444 Miami, Florida stations.

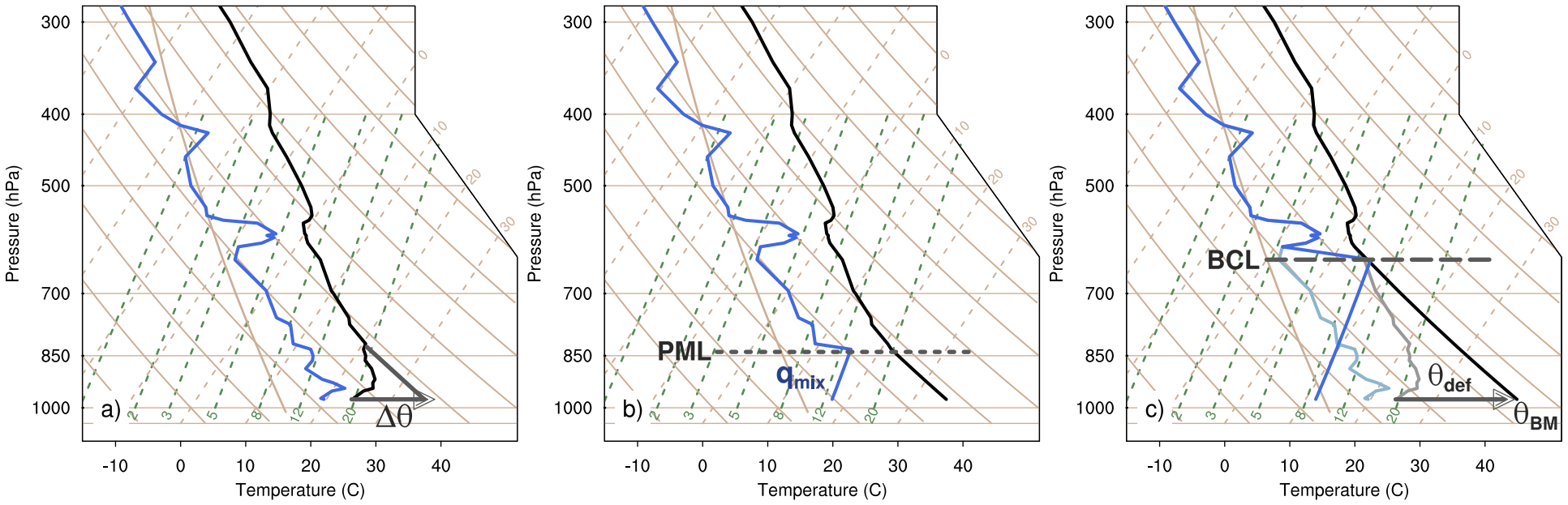
Pressure (hPa)
300
400
500
700
850
1000
-10
0
10
20
30
40
Temperature (C)
a)
Δθ
b)
PML
q_{mix}
c)
BCL
θ_{def}
θ_{BM}

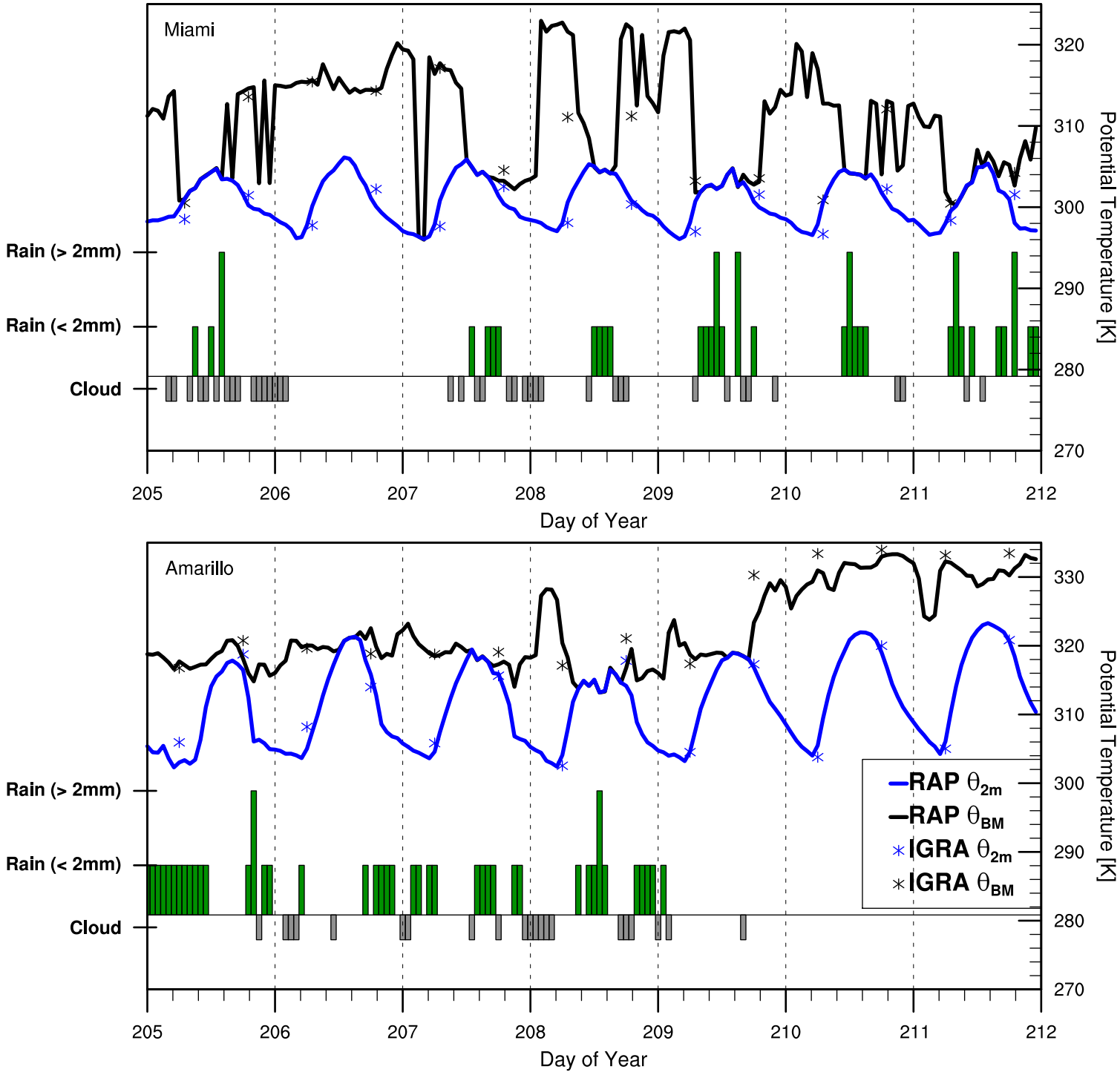
Miami
Rain (> 2mm)
Rain (< 2mm)
Cloud
320
310
300
290
280
270
Potential Temperature [K]
205
206
207
208
209
210
211
212
Day of Year
Amarillo
Rain (> 2mm)
Rain (< 2mm)
Cloud
330
320
310
300
290
280
270
Potential Temperature [K]
RAP θ2m
RAP θBM
IGRA θ2m
IGRA θBM
205
206
207
208
209
210
211
212
Day of Year

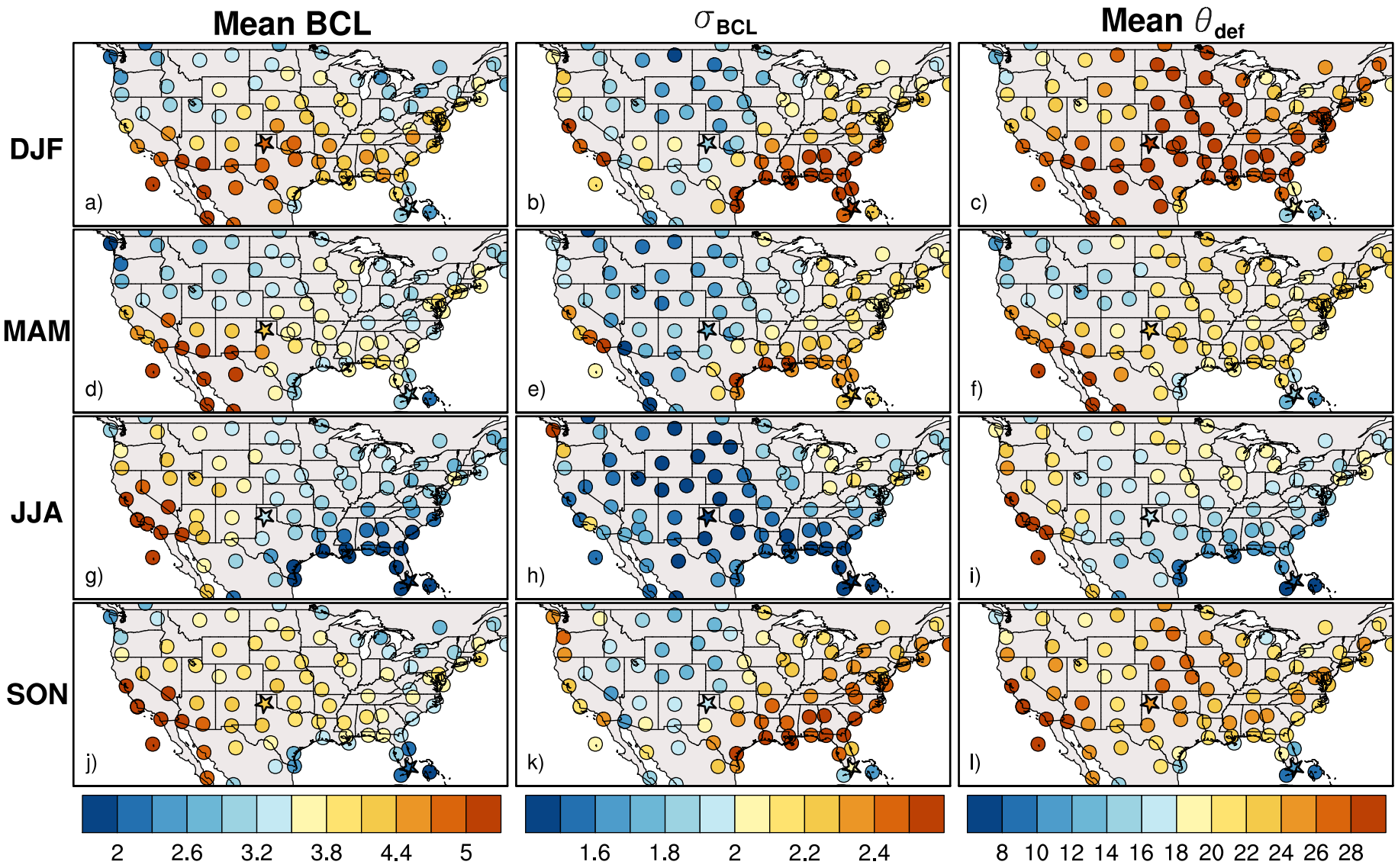
Mean BCL
σ_{BCL}
Mean θ_{def}
DJF
MAM
JJA
SON
a)
b)
c)
d)
e)
f)
g)
h)
i)
j)
k)
l)
2 2.6 3.2 3.8 4.4 5
1.6 1.8 2 2.2 2.4
8 10 12 14 16 18 20 22 24 26 28